Carbon 153 (2019) 458–466

Contents lists available at ScienceDirect

Carbon

journal homepage: www.elsevier.com/locate/carbon

Hydrogen sieving from intrinsic defects of benzene-derived single-layer graphene

Majharul Haque Khan, Mina Moradi, Mostapha Dakhchoune, Mojtaba Rezaei, Shiqi Huang, Jing Zhao, Kumar Varoon Agrawal*

Laboratory of Advanced Separations (LAS), École Polytechnique Fédérale de Lausanne, (EPFL), Sion, Switzerland

ARTICLE INFO

Article history:
Received 12 April 2019
Received in revised form
18 June 2019
Accepted 13 July 2019
Available online 13 July 2019

ABSTRACT

Single-layer graphene films, crystallized by chemical vapor deposition, host a low density of vacancy defects that are attractive for the size-sieving of molecules. The size and the density of such defects are a function of the growth temperature and the carbon precursor. So far, the studies applying the intrinsic defects of graphene have only used CH_4 as the precursor. Since there are reports claiming the synthesis of graphene from benzene at low temperature (up to 100 °C on Cu foil), we systematically studied the crystallization of benzene-derived graphene and the evolution of intrinsic defects. We demonstrate that graphene cannot grow from benzene below 700 °C on Cu. We attribute the reports on low-temperature growth of graphene to the practice of pre-annealing of the Cu foil at 1000 °C and to the unintentional benzene residues in the reactor if the reactor is not purged carefully. Finally, we report that high-quality single-layer-graphene can be synthesized using benzene above 825 °C. The majority of vacancy defects in benzene-derived graphene (900–1000 °C) are smaller than 0.38 nm, leading to an attractive H_2 sieving (H_2 permeance over 2000 gas permeation units; H_2/C_3H_8 and H_2/SF_6 selectivities of 12 and 50, respectively).

1. Introduction

A facile crystallization of single-layer graphene by the chemical vapor deposition (CVD) process has made it possible to apply graphene for a number of applications [1,2]. Nanoporous single-layer-graphene membranes are especially appealing for the size-sieving applications because, at the limit of the film thickness, pores incorporated in the graphene lattice offer the least resistance to the molecular transport [3–5]. Since the size of these pores determines the molecular selectivity, several research groups have attempted to control the size by controlling the way they are incorporated in the graphene lattice. A popular route is controlled etching of the graphene lattice, e.g. by focused-ion beam [3], UV/ozone based etching [6,7], electron irradiation [8], plasma/ozone [9], etc. For example, Bunch and co-workers reported angstrom-sized pores in mechanically-exfoliated graphene by using ultraviolent light induced oxidation [10]. Karnik and co-workers reported molecular sieving defects with a density of ca. 10^{-11} cm^{-2} using a combination of ion-bombardment and oxygen plasma [11]. Interestingly, CVD graphene hosts a small density of subnanometer-sized intrinsic vacancy-defects, incorporated during the crystallization stage, which by themselves can be attractive for molecular sieving. For example, recently, we showed that intrinsic defects with density of ~10^{10} cm^{-2} in methane-based CVD graphene can sieve H_2 from the larger gas molecules [12]. Kidambi et al. demonstrated that intrinsic defects in graphene, synthesized at a lower temperature (CVD of CH_4 at 850–950 °C), can differentiate hydrated K^+ and Cl^- ions from molecules that are larger than 1 nm in size [13]. Since the intrinsic defects are dependent on the crystallization conditions, mainly the chemical composition of growth precursor, precursor concentration, growth temperature, etc., changing the crystallization conditions can change the density and the size of the intrinsic defects. For membrane application, such experiments must be carried out in a way that yields high-quality, pinhole-free graphene. However, the growth of high-quality, fully-intergrown single-layer-graphene either at low temperature or using a carbon precursor other than methane is challenging.

Graphene growth at a temperature significantly lower than 1000 °C requires a hydrocarbon precursor that possesses faster dehydrogenation kinetics than methane [14]. In this context,

* Corresponding author.
E-mail address: kumar.agrawal@epfl.ch (K.V. Agrawal).

https://doi.org/10.1016/j.carbon.2019.07.045

aromatic precursors like benzene [14–17], pyridine [18], pyrene [19], hexabromobenzene [20], pentachloropyridine [21], *p*-terphenyl [14,22] have been reported. In addition, plasma-enhanced CVD has been also reported where plasma dissociates the carbon-hydrogen bond at the low temperature [23,24]. In a recent study, graphene was successfully grown at 100 °C on polycarbonate using molten gallium as a catalyst and methane as a precursor [25]. However, none of these studies yield high-quality graphene essential for the fabrication of a gas separation membrane. For instance, the reported graphene was either not fully intergrown [16], or was extremely defective, doped and multilayered [15,20,21]. Even then, a 1000 °C annealing of the Cu foil is almost always implemented to remove the oxide layer on Cu and to smoothen the surface [14–16,21,22,26].

Benzene is one of the most investigated aromatic precursors for graphene growth at temperature down to 100 °C [14–16]. Herein, we have systematically investigated graphene growth using benzene as the carbon precursor in the temperature range of 400–1000 °C. Based on more than two hundred experiments, we confirm that benzene cannot yield graphene below a growth temperature of 700 °C. Further, we show that graphene growth can occur when the Cu foil, the catalytic support for graphene, is annealed at 1000 °C and when benzene residues from prior experimental runs are not effectively removed the reactor. We believe that this could be the primary reason behind several reports on benzene growth at the temperature below 700 °C because all such reports used Cu annealing at 1000 °C prior to the low-temperature graphene growth. Finally, we optimized the growth of high-quality single-layer graphene using benzene in the temperature range of 825–1000 °C and report that the majority of vacancy-defects in the resulting graphene lattice are molecular-sized yielding an attractive hydrogen sieving (H_2/C_3H_6 and H_2/SF_6 selectivities of 12 and 50, respectively, with H_2 permeance over 2000 gas permeation unit or GPU; 1 GPU = 3.35×10^{-10} mol m^{-2} s^{-1} Pa^{-1}) from millimeter-sized graphene domains.

2. Experimental

2.1. Graphene growth with benzene

Cu foil (0.025 mm thick, 99.98% purity, Sigma Aldrich) was pretreated in acetone and isopropanol before CVD. Anhydrous benzene (99.8%, Sigma Aldrich) was used as a precursor for graphene growth in a low-pressure CVD (LPCVD) system. For growth studies above 825 °C, Cu foil was annealed at the growth temperatures for 30 min under 50 sccm CO_2 and 10 sccm H_2 to remove the organic contaminants and surface oxides from the Cu surface. For growth studies below 825 °C, the Cu foil was annealed at 1000 °C for 30 min either in a separate benzene-free setup or in the benzene CVD setup ensuring complete removal of benzene residues before the Cu annealing step. Benzene can condense along the tubing connected to the CVD reactor. Therefore, prior to each experiment, the tubing was heated at 100 °C for 30 min under vacuum while the CVD setup was connected to a liquid nitrogen trap to completely remove the residual benzene in the reactor.

Graphene growth was carried out by the LPCVD process at a total pressure of 90 mTorr. The H_2 flow rate was kept at 10 sccm while the benzene partial pressure inside the CVD system was finely controlled using a metering valve (Fig. S1). After the graphene growth, the benzene valve was closed and the furnace was cooled down to near room temperature under the H_2 atmosphere.

2.2. Graphene transfer for membrane fabrication

The membrane fabrication process followed the procedure described in another study [12]. Briefly, a solution was prepared by dissolving 0.1 g block copolymer (poly (styrene-*b*-4-vinyl pyridine) and 0.2 g turanose in dimethylformamide (DMF). The solution was aged in an autoclave at 180 °C for 3 h. The aged solution was spin-coated on graphene at 2000 rpm for 2 min. Pyrolysis of the coated film was carried out at 500 °C in a reducing atmosphere of H_2/Ar for 1 h leading to the nanoporous carbon (NPC) film. The underlying Cu foil was etched away using 0.5 M ammonium persulfate solution by floating the NPC coated graphene/Cu foil on top of the solution. The NPC coated graphene was subsequently transferred to deionized water bath several times to rinse the underside of graphene from the residues of the etching bath. A 50-μm-thick W foil drilled with 5 μm sized holes in 1 mm^2 area (Potomac Photonics Inc.) was used as a macroporous substrate for scooping out the NPC-reinforced graphene film to obtain the membrane.

2.3. Permeation test

For the gas permeation test of the single component gases across the graphene membrane, a homemade permeation cell was prepared [12,27,29]. Permeation measurements were done in a dead-end mode; i.e., the valve at the retentate side was kept closed. During the test, a total pressure difference of 1 bar was maintained between the feed and the permeate side. The W substrate, supporting the NPC-reinforced graphene, acted as a gasket for ensuring leak-tight sealing in the VCR fittings (Swagelok) equipped membrane module. The membrane module was kept inside an oven for ensuring temperature uniformity and ease of heating at different temperatures. Before testing, each membrane was first preheated at 150 °C for removing the atmospheric contaminants. Single component gas permeance was measured for H_2, CH_4, C_3H_8, and SF_6. Argon at 1 bar was used to sweep the permeate into the mass spectrometer (Hiden Analytical, HPR-20) and the real-time data was recorded. The gas permeation data was analyzed from the average of the steady-state portion of the permeation data. The steady-state was typically obtained within 30 min when the permeation conditions were changed (temperature, feed gas, etc.).

2.4. Graphene transfer to Si wafer and TEM grid

Graphene was transferred to Si wafer hosting a 300 thick SiO_2 layer and ultrathin carbon coated transmission electron microscopy (TEM) grid using the conventional poly(methyl methacrylate) or PMMA-assisted transfer method [30]. Typically, PMMA solution in anisole (950 PMMA, Microchem) was spin-coated on as-synthesized graphene at 2000 rpm for 1 min. The Cu foil supporting PMMA coated graphene was floated on 0.5 M ammonium persulfate solution. After etching Cu, the floating PMMA coated graphene film was transferred to deionized water bath several times. Subsequently, the film was scooped out with the substrates and was placed under vacuum for a few minutes to remove the water film trapped between graphene and the substrates. Finally, the PMMA layer was removed by heating under Ar/H_2 atmosphere at 500 °C for 1 h.

2.5. Characterization

Optical microscopy images were taken in MM500T advanced metallurgical microscope. Scanning electron microscope (SEM) images were obtained in FEI Teneo scanning electron microscope using a working distance of 3–6 mm and operating voltage of 1–2 kV to reduce the electron beam induced charging of the graphene. Reinshow inVia™ confocal Raman spectroscopy instrument equipped with 457 nm laser wavelength was used for the characterization of defects in graphene. The laser power was kept below

2 mW to reduce the localized heating in graphene. 100x objective lens yielding a spot size of ca. 600 nm was used. Dark field TEM (DF-TEM) images and selected area electron diffraction (SAED) patterns were obtained in FEI Tecnai G2 Spirit Twin transmission electron microscope at the operating voltage of 120 kV.

3. Results and discussion

The CVD system for graphene growth comprised of a tubular furnace hosting a pre-cleaned Cu foil and connected with a H_2 and a benzene delivery system (Fig. 1). Benzene was supplied from a homemade reservoir equipped with a calibrated metering valve, which allowed precise control of benzene concentration (2–30 mTorr, Fig. S1) in the growth chamber.

Our initial results on benzene-based graphene crystallization seemed to verify the literature report that a high-quality single-layer graphene (I_{2D}/I_G of 3.07 ± 0.47) with a low density of intrinsic defects (I_D/I_G of 0.075 ± 0.03) and a grain size of 10 μm can be grown at temperature as low as 400 °C (Fig. 2a–b, S2) [14–16]. The resulting graphene film covered the entire Cu surface and typical wrinkles in the graphene film on Cu could be observed (Fig. 2b). However, after careful observations of the subsequent growth experiments, we discovered that residual benzene in the CVD reactor after each experiment was responsible for the graphene growth, and graphene grew only when the Cu foil was annealed at 1000 °C in the presence of these unintentional residues. In general, graphene growth was observed in the contaminated CVD setup when the Cu foil was annealed at 1000 °C even without the subsequent synthesis step (Fig. S3). When the Cu foil was not annealed in the CVD furnace with residues, graphene was not obtained at the low temperature. Moreover, when the Cu foil was annealed in a separate CVD system free from benzene, graphene was not obtained at the low temperature. Subsequently, after each experiment, the CVD reactor connected to the benzene reservoir was cleaned from the benzene residues using a liquid nitrogen trap, effectively condensing most of the benzene residues in the cold trap. After this cleaning step, the extent of graphene crystallization was visibly reduced at 400 °C, and only islands of graphene were observed covering only 1% of the surface of the Cu foil (Fig. 2c–e). Most of the Cu surface was covered with a layer of amorphous carbon (Fig. 2f). When the benzene residues were completely eliminated by preheating the gas/vapor delivery lines and the cold section of the reactor, in addition to the liquid nitrogen trap method, we did not observe any graphene growth at 400 °C, and only amorphous carbon was detected by Raman spectroscopy (Fig. 2g and h).

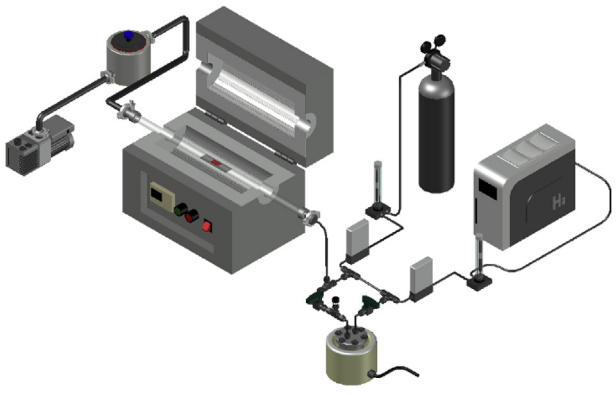

Fig. 1. A schematic of the setup for the synthesis of single-layer graphene using benzene. High purity (99.99%) H_2 and CO_2, were supplied from a hydrogen generator and gas cylinder, respectively, and were further purified by an adsorbent column for O_2, H_2O, and hydrocarbon. Gas flow was controlled by mass flow controllers. A controlled partial pressure of benzene was established with a homemade setup using a calibrated metering valve. A cold trap was used in the downstream of the CVD setup to condense residual benzene, preventing its entrance in the vacuum pump. (A colour version of this figure can be viewed online.)

To identify the lowest growth temperature using benzene as a precursor, we carried out a systematic graphene growth study in the temperature range of 400–1000 °C on Cu substrate ensuring that either the Cu was annealed in a separate benzene-free reactor or the benzene residues were effectively purged from the reactor before the experiment (Fig. 3a). Based on this, we report that the lowest temperature to obtain high-quality graphene film using benzene, without requiring Cu pre-annealing at 1000 °C, is 825 °C (Fig. 3). Below this temperature, without Cu pre-annealing at 1000 °C, graphene could not be crystallized. Even with the Cu pre-annealing at 1000 °C, graphene could not be crystallized below 700 °C, and only amorphous carbon was deposited on Cu. At 750 and 700 °C, highly defective and discontinuous graphene domains were formed (Figs. S4 and S5). The successful growth of high-quality graphene films at 825 °C, while avoiding the pre-annealing of Cu foil at 1000 °C, reduces the energy and equipment requirements for the synthesis of graphene.

The pre-annealing assisted in smoothening the foil-rolling-induced roughness and removing the native oxide layer in the as-received Cu surface, which otherwise could not be completely removed at a temperature below 825 °C (Fig. 3b and c). The annealed foils were stored and were subsequently used for graphene growth from benzene without any further annealing. In the absence of pre-annealing, only amorphous carbon was observed at 800 °C (Fig. 3c, e). With the help of pre-annealing, single-layer graphene with I_D/I_G of 0.43 ± 0.05 and I_{2D}/I_G of 1.47 ± 0.28 could be crystallized at 800 °C (Fig. 3d). The entire Cu surface seemed to be covered with graphene, and the typical wrinkles of graphene could be observed (Fig. S6). However, occasionally, micron-sized gaps in the graphene film were found (Fig. S7), making the 800 °C sample unsuitable for the molecular-sieving application. Therefore, for the fabrication of membranes, the graphene growth studies were restricted in the growth temperature range of 825–1000 °C.

Continuous graphene films were formed when the growth was carried out at 1000, 900, and 825 °C for 30 min (Fig. 4). At 1000 °C, micron-sized multilayered graphene domains, covering 6% of the area, were observed (Fig. 4a). The white particles seen in Fig. 4b and c are SiO_x particles (Fig. S8), which are commonly observed for the CVD graphene grown on Cu foils inside the fused silica reactors. These SiO_x particles originate from the fused silica tube. One of the commonly cited hypotheses on the origin of SiO_x particle is that the high temperature generated Cu vapors can diffuse inside the fused silica along the silica phase transition zone (α to β silica phase transition). The intrusion of copper causes the precipitation of SiO_x nanoparticles, which in turn reaches the Cu catalyst surface and deposit there [31,32]. Nevertheless, we did not observe any large holes or cracks in graphene due to these particles, which helped us fabricating gas-selective membranes as discussed later.

Raman spectroscopy study on these samples was carried out to identify the quality, thickness, and homogeneity of the as-grown graphene. Raman mapping images were obtained from 20×20 μm area, directly on the Cu substrate, using a raster size mapping from 1100 to 3200 cm^{-1}. The average I_{2D}/I_G ratio was significantly lower in 1000 °C grown sample ($I_{2D}/I_G = 1.4 \pm 0.15$) compared to the 900 and 825 °C grown sample ($I_{2D}/I_G = 2.35 \pm 0.25$ and 1.91 ± 0.18, respectively, Fig. S9). This can be attributed to the presence of multilayer graphene at 1000 °C grown sample. On the other hand, the defect density was lower in the 1000 °C grown sample ($I_D/I_G = 0.08 \pm 0.02$), confirming that high-quality graphene could be grown using benzene (Fig. 4d). The defect density increased with lowering the growth temperature ($I_D/$

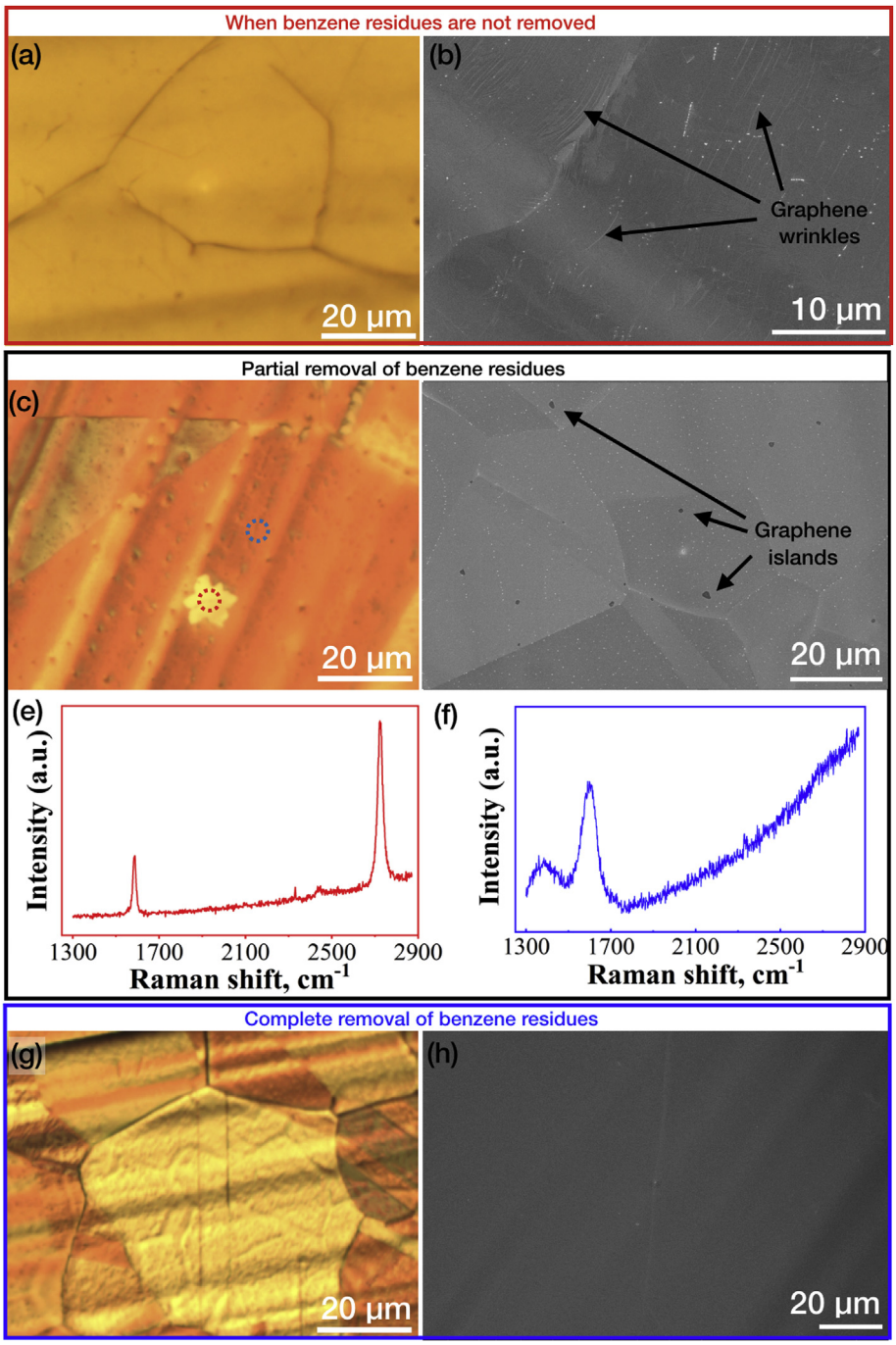

Fig. 2. Role of the unintentional benzene residues inside the CVD system when the Cu foil is annealed at 1000 °C before the graphene growth. When the benzene residues were not removed, a complete surface coverage of Cu with a polycrystalline graphene film was observed as shown in optical (a) and SEM image (b). When the benzene residues were partially removed using the liquid nitrogen trap, only isolated graphene grains were observed as shown in optical (c) and SEM image (d). The graphene grains, highlighted with the red circle in panel (c), were single-layer as indicated by Raman spectra in (e). Regions not covered by graphene, highlighted with the blue circle in panel (c), had a layer of amorphous carbon as indicated by Raman spectra in (f). Finally, when the benzene residue was completely removed using the liquid nitrogen trap and the heating of inlets and outlets, no graphene growth was observed as shown by optical (g) and SEM image (h). To visualize graphene in optical images, Cu foils were heated in air at 200 °C. (A colour version of this figure can be viewed online.)

$I_G = 0.14 \pm 0.05$ and 0.35 ± 0.1 at 900 and 825 °C, respectively, Fig. 4e and f). Based on the carbon amorphization trajectory, [33,34] the defect density for growth at 1000, 900, and 825 °C were ca. 3.6×10^{10}, 5.8×10^{10} and 1.5×10^{11} cm^{-2}, respectively, and the distance between defects, L_D, were ca. 30.0, 23.7 and 14.9 nm, respectively (Supplementary Note 1). Interestingly, continuous single-layer graphene could be crystallized within 1 min of growth at 825–1000 °C (I_{2D}/I_G of 1.89 ± 0.14, 2.3 ± 0.15, 1.35 ± 0.22 for 1000, 900, and 825 °C, respectively, Fig. S10). We note that this growth was exclusively because of the 1 min of benzene exposure as the residual benzene from previous runs was removed. The defect density, however, was higher in these samples compared to those grown for 30 min (I_D/I_G of 0.15 ± 0.03, 0.25 ± 0.06, 0.39 ± 0.15 for growth at 1000, 900, and 825 °C, respectively) perhaps because of

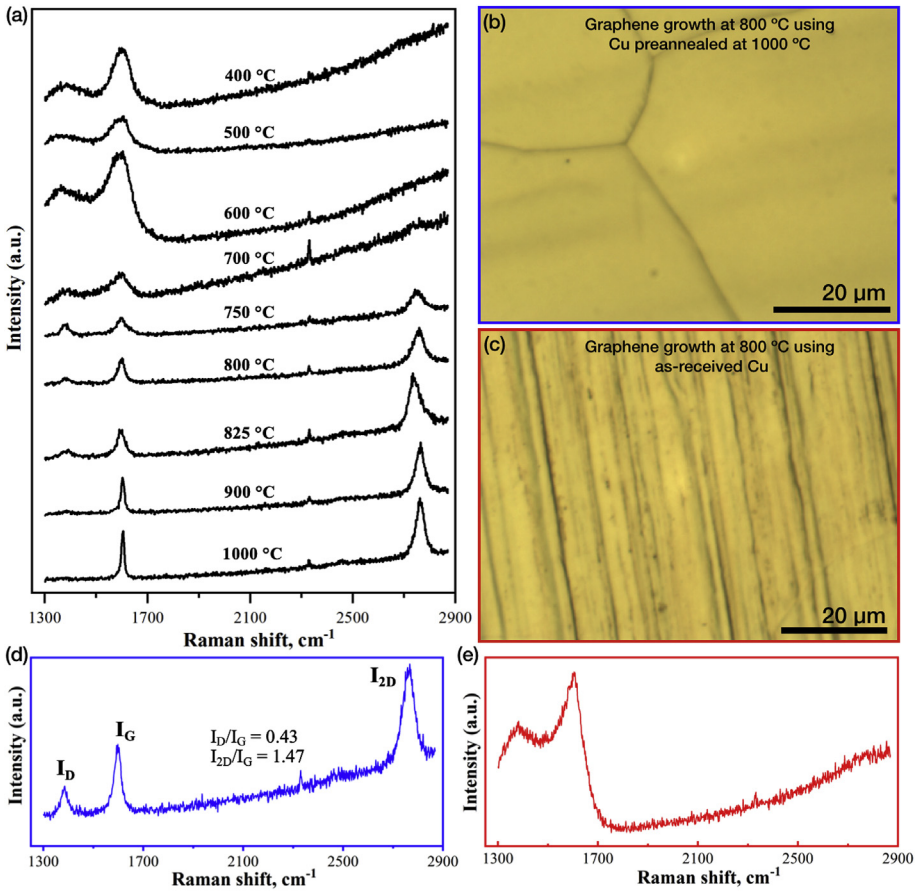

Fig. 3. (a) Representative Raman spectra of benzene-derived graphene at various growth temperatures (400–1000 °C). Cu was pre-annealed at 1000 °C in a residue-free setup for growth below 825 °C. For growth above 825 °C, the Cu annealing was carried out at the growth temperature. Optical images of samples obtained from 800 °C growth when the Cu foil was pre-annealed, and (b) when the Cu foil was not pre-annealed at 1000 °C (c). Characteristic Raman spectra from (b) and (c) are shown in (d) and (e), respectively. (A colour version of this figure can be viewed online.)

an incomplete grain coalescence in the former case. This implies that a longer growth time annealed lattice defects, most likely by improving the grain intergrowth.

Dark field-transmission electron microscopy (DF-TEM) was carried out to determine the grain size of the graphene (Fig. 4g–i and S11) [28]. The images representing separate grains were false-colored and superimposed on top of each other to understand the size and orientation of graphene grains as a function of the growth temperatures. Grains larger than 20 μm dominated the sample grown at 1000 °C and 900 °C (Fig. 4g–h, S11a-f). There were, however, several sub-1-μm grains for the 900 °C sample (Fig. 4h, S11d-f). At 825 °C, all grains were 1–2 μm in size (Fig. 4i, S11g-j).

3.1. Can graphene grow from benzene at growth temperature below 500 °C?

The commonly cited growth mechanism of benzene-derived graphene on Cu foil at temperature below 700 °C follows (i) adsorption of benzene on the Cu surface by the London dispersion force, (ii) dehydrogenation of benzene followed by diffusion of dehydrogenated carbon rings on the Cu surface leading to the formation of nuclei [14–16]. However, benzene is thermally stable against decomposition at least up to 600 °C, and up to 550 °C in the presence of Cu catalyst [35]. No dehydrogenation products were reported below this temperature [35]. Therefore, the crystallization of graphene domains at a temperature lower than 500 °C is unlikely. This implies that the graphene observed in these low-temperature studies must have an origin in the unintentional growth during the Cu foil annealing in the presence of benzene residues, as demonstrated in this study.

At high temperature (825–1000 °C), benzene molecules can spontaneously degrade and self-dehydrogenate yielding carbon radicals (partially dehydrogenated benzene, biphenyl, etc.) in the gas phase. These carbon radicals are expected to act as graphene precursor in addition to those radicals which are generated by partial dehydrogenation of benzene on Cu [35]. Since Cu has a low carbon solubility at high temperature (0.04% at 1000 °C) [36], the graphene nucleation and growth mediated by Cu is expected to take place on the Cu surface. The crystallization likely proceeds by nucleation at an active Cu site where the critical carbon cluster size, formed by the merger of carbon radicals, becomes stable at the CVD conditions. The nucleus is then expected to grow both by addition of adsorbed precursor diffusing on the surface of Cu, as well as from the precursors adsorbing from the gas phase. In this fashion, the generation of carbon radicals in the gas phase by spontaneous degradation of benzene could accelerate graphene nucleation and growth. This is evidenced from the fact that a continuous graphene film could be grown within 1 min of benzene exposure at 825–900 °C (Fig. S10), which is usually not the case when methane is used as the carbon precursor. The observation of bi- and trilayer graphene at 1000 °C can also be attributed to the significant amount of these carbon radicals in the gas phase at 1000 °C [35].

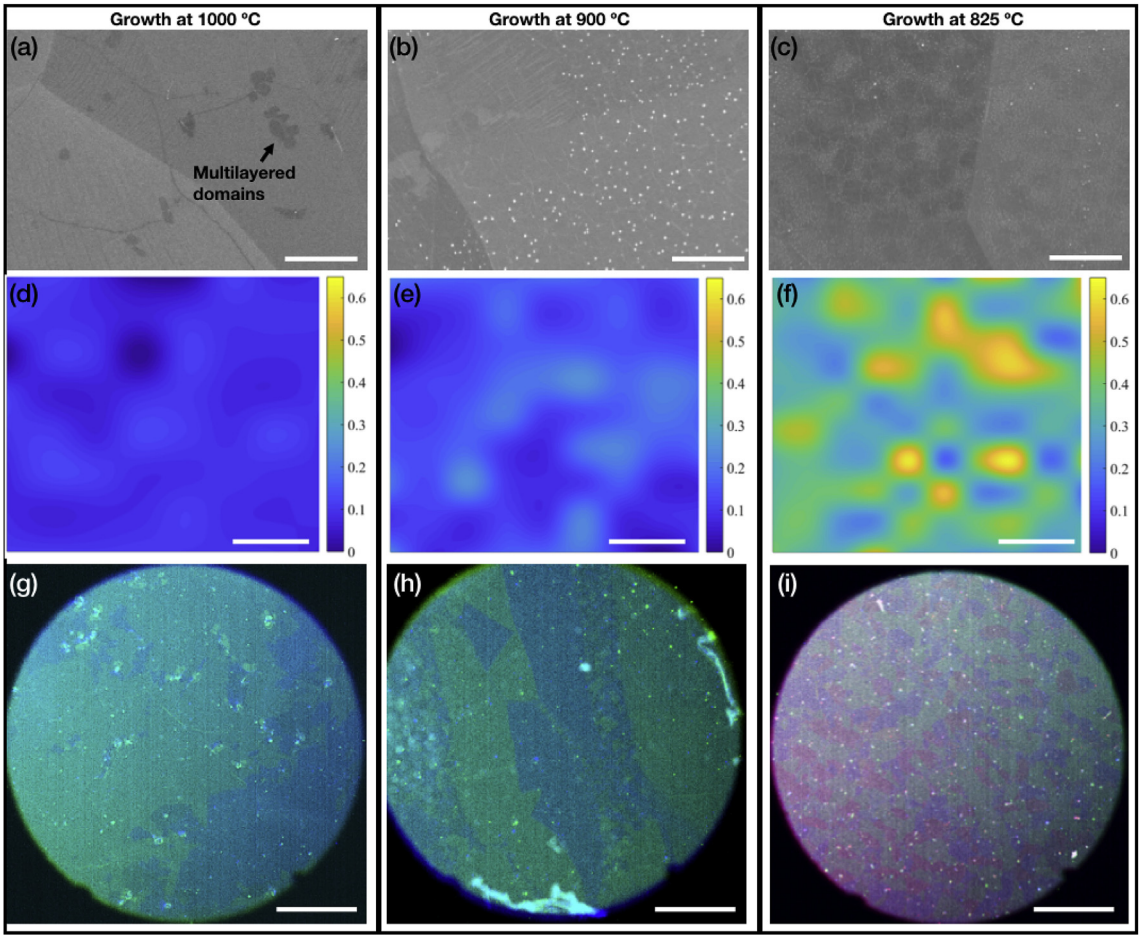

Fig. 4. Characterization of benzene-derived graphene grown at 825–1000 °C for 30 min. SEM images of graphene grown at 1000, 900 and 825 °C are shown in (a), (b) and (c), respectively. Corresponding Raman I_D/I_G mapped images from 20 × 20 μm area are shown in (d), (e) and (f), respectively. (g–h) False-colored DF-TEM images revealing the effect of temperature on the grain size and the orientation. Graphene grains are colored green and blue in (g) and (h) resembling two separate orientations. In (i), three separate orientations can be identified from red, green and violet domains. The scale bars in the images correspond to 5 μm. (A colour version of this figure can be viewed online.)

3.2. Understanding the size of intrinsic defects by gas transport experiments

$1 \times 1\ mm^2$ sized graphene membranes were fabricated on top of a perforated tungsten disk using the nanoporous carbon (NPC) film assisted transfer process (details in the methods, Fig. S12) [12]. The NPC film hosting 20–30 nm pores mechanically reinforces graphene and eliminates cracks and tears during the transfer of graphene from Cu to a porous substrate. The thickness of NPC film was kept low, at less than 100 nm, to ensure that the gas transport resistance across the NPC film is low (Fig. S13). The graphene film was intact after the transfer to the tungsten substrate and no apparent cracks or tears were found. This enables a direct characterization of molecular transport through the graphene nanopores, otherwise, the presence of cracks in graphene film leads to a transport which can be dominated by cracks. In such cases, one requires complicated post-transfer defect sealing technique to reduce the transport through defects [37,38]. Graphene with NPC film on top was found to closely follow the surface topography of the Cu foil. Therefore, the grain boundaries and steps of the Cu surfaces were imprinted on the NPC coated graphene film after the transfer (Fig. S12b). The transferred graphene film could withstand up to 8 bar of transmembrane pressure difference, the pressurization limit in our setup, without generating any tear or crack in the membrane. Gas permeance measurements were carried out with a transmembrane partial pressure difference of 2 bar (details in method).

Permeation mechanism of gas molecules across two-dimensional nanopores depends on the size of the nanopores [39–42]. Typically, the gas-phase effusive transport is dominant for a nanopore that is significantly larger than the molecular size. Typically Knudsen selectivity (inverse of the square root of the ratio of the molecular weights) is observed if the pores are smaller than the mean free path of the molecules [3]. On the other hand, adsorbed-phase surface transport is dominant for the nanopores that are commensurate to the molecular size. Temperature-activated transport characterizes adsorbed-phase transport when the electron-density-gap in the pore is comparable to the kinetic diameter of the molecule [4]. To understand the nature and transport property of intrinsic defects in graphene crystallized at 1000, 900, and 825 °C, single component permeance measurements were carried out using four gases (H_2, CH_4, C_3H_6, and SF_6) at three different permeation temperatures (30, 100 and 150 °C).

For 1000 and 900 °C samples, six membranes were prepared, three for each growth temperature. The permeance for all four gases increased with increasing the permeation temperature indicating that the transport was in the temperature-activated regime (Fig. 5a, c and S14; Tables S1 and S2). The activation energies of H_2 for the 1000 and 900 °C samples were comparable at 8.6 ± 1.5 and 10.4 ± 0.4 kJ/mol, respectively (Supplementary Note 2,

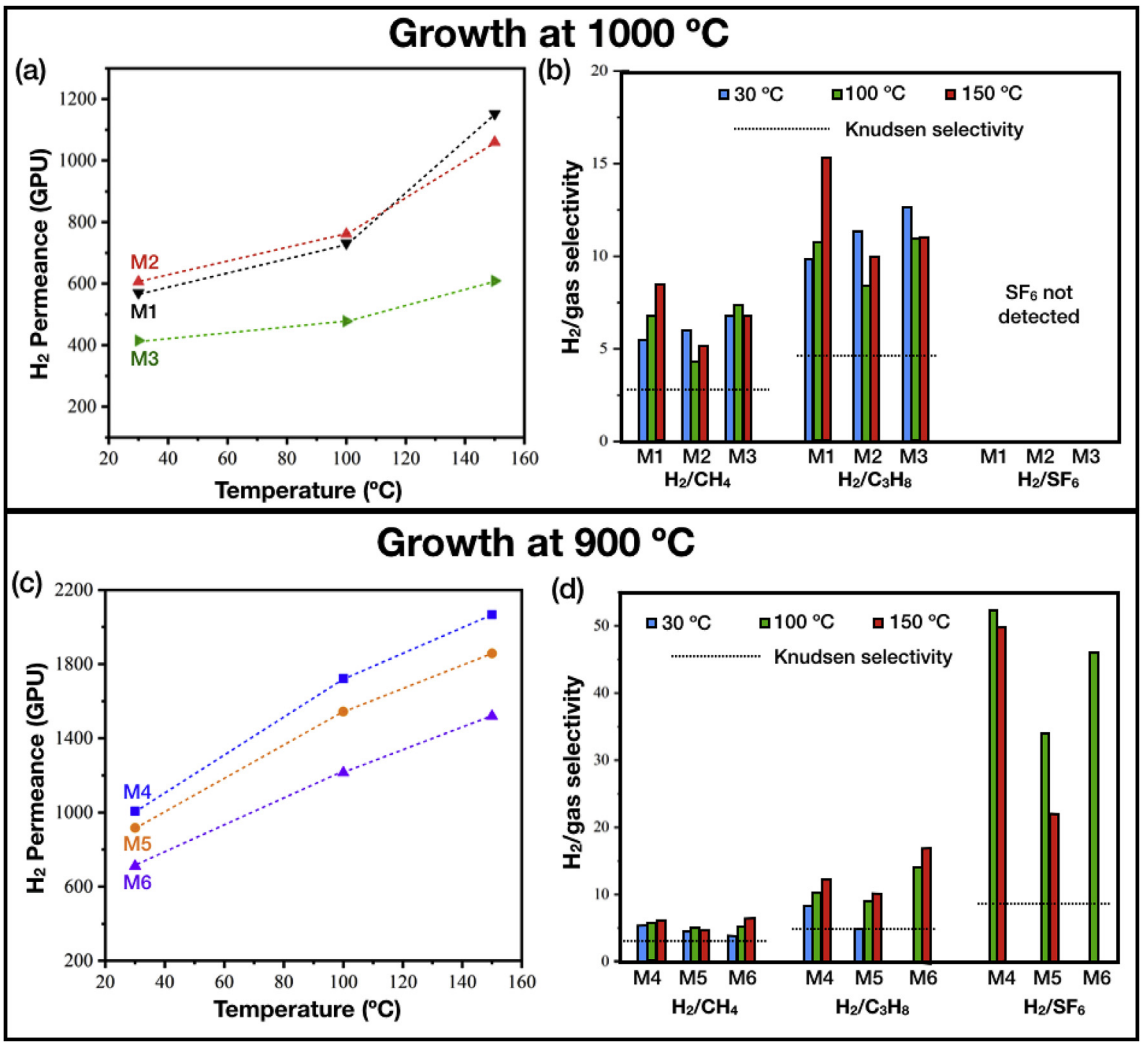

Fig. 5. Single-component gas permeation and selectivity data from benzene-derived graphene. Permeation of H_2, CH_4, C_3H_6, and SF_6 as a function of permeation temperature is shown in (a) for growth at 1000 °C, and in (c) for growth at 900 °C. Corresponding gas selectivities with respect to H_2 are shown in (b) and (d), respectively. (A colour version of this figure can be viewed online.)

Tables S3 and S4). Generally, the transport of molecules through graphene nanopores is temperature-activated if the nanopores are equal in size or slightly smaller than the size of the molecules [42]. In this case, the energy-barrier for the gas molecules to diffuse across the nanopores manifests itself as the activation energy in the permeation experiments. So, a decrease in the activation energy for a particular molecule indicates a larger pore size [10]. We note that the activation energies for H_2 in this study are much smaller than that reported (20.2 ± 2.7 kJ/mol [12]) for the hydrogen transport from the intrinsic defects of methane-derived graphene, consistent with the fact that intrinsic defects in benzene-derived graphene are expected to be slightly larger than those when graphene is derived from CH_4 attributing to a smaller size of precursor radicals for the latter. Using density functional theory, Jiang and coworkers calculated an activation energy of 0.22 eV (21 kJ/mol) for the translocation of H_2 from hydrogen-functionalized pore-10. Therefore, the intrinsic defects in benzene-derived graphene must be larger than pore-10 [4].

Overall, we observed the size-sieving phenomenon, and activation energies increased sharply as a function of molecular size (Tables S3 and S4). The majority of the pores were smaller than 0.38 nm, the kinetic diameter of CH_4. The permeance followed the trend $H_2 \gg CH_4 > C_3H_8 > SF_6$, leading to attractive gas selectivities with H_2/CH_4, H_2/C_3H_8 and H_2/SF_6 selectivities exceeding their corresponding Knudsen selectivities of 2.8, 4.7, and 8.5, respectively, by a significant margin (Fig. 5b, d). For example, the highest H_2/CH_4 and H_2/C_3H_8 selectivities at 1000 °C were 8.4 and 15.3, respectively, and SF_6 was not detected in the permeate side. On the other hand, the highest H_2/CH_4, H_2/C_3H_8, and H_2/SF_6 selectivities at 900 °C were 6.3, 16.9, and 52. The combination of high H_2 permeance and gas selectivity for graphene grown at 900 °C makes benzene-derived graphene highly attractive. For example, at 150 °C, the membrane M4 yielded H_2 permeance of 2000 GPU with the corresponding H_2/CH_4, H_2/C_3H_8 and H_2/SF_6 selectivities of 6.1, 12.2 and 49.8, respectively.

These selectivities are lower compared to those obtained from carefully etched graphene. For example, Bunch and coworkers reported H_2/CH_4 selectivity close to 1000 from their Bi-3.4 membrane [6]. This can be attributed to a higher percentage of nanopores operating in the effusive transport mode in the benzene-derived graphene. Using permeation coefficients of 10^{-22} and 10^{-26} mol s^{-1} Pa^{-1} for H_2 and for larger molecules (CH_4, C_3H_8 and SF_6), respectively, an analysis for the membrane M4 revealed that the population of pores larger than 0.38, 0.43, and 0.55 nm were 86, 62

and 21 ppm, respectively (Supplementary Note 3 and Table S5). Since the permeation coefficients are sensitive to the electron-density-gap of the pore, therefore, an additional comparison based on the H_2/CH_4 selectivity was carried out. For example, changing permeation coefficient of CH_4 from 10^{-26} mol s^{-1} Pa^{-1} to a wide range (10^{-24} to 10^{-27}) while fixing that of H_2 to 10^{-22} mol s^{-1} Pa^{-1} did not change the result significantly (ppm of pores larger than 0.38 nm ranged from 34 to 86 ppm; Table S6). However, when the permeation coefficient of H_2 was increased to 10^{-21} mol s^{-1} Pa^{-1}, the resulting ppm of effusive pore increased to 862, which indicates that membrane could tolerate a higher population of defects.

Higher H_2 permeance for the graphene grown at 900 °C compared to that for graphene grown at 1000 °C is consistent with the higher density of the intrinsic defects in the former case. These intrinsic defects are likely generated as a consequence of an imperfect addition of the carbon radicals (for example, dehydrogenated benzene ring) to the growing graphene lattice. Imperfect coalescence of graphene grains would also give rise to such vacancy defects. When the growth temperature was reduced to 825 °C, an extremely high H_2 permeance was achieved (close to 5000 GPU), however, the gas selectivities were comparable to the corresponding Knudsen selectivities (for example: 4.3, 5.7, and 9.5 for H_2/CH_4, H_2/C_3H_8 and H_2/SF_6, respectively, at 150 °C; Table S7). The high permeance can be attributed to a relatively higher defect density (1.46×10^{11} defects/cm^2) and small grain sizes (1–2 μm) in this sample. Low gas selectivities from these samples highlight that a minuscule concentration of defects in two-dimensional membranes can have a significant impact on gas selectivity attributing to extremely high permeation coefficient of the effusive transport in comparison to that for the activated transport. A slow growth (long growth time with a smaller benzene concentration) may improve the quality of graphene at 825 °C. The slight variation in gas selectivity among the three batches of membranes can be attributed to the varying percentage of non-selective intrinsic defects from one batch to another batch.

Finally, we note that the gas selectivity observed here was solely because of the intrinsic defects in graphene and not because of the NPC film. The latter primarily served the role of high-permeance mechanical reinforcement. The gas permeance through the standalone NPC film, without the graphene film, is orders of magnitude higher than that obtained with the graphene film in this study (Table S8), while the gas selectivity from NPC regime corresponds to the Knudsen selectivity attributing to the 20–30 nm sized pores of the NPC film [12].

4. Conclusion

In conclusion, we investigated the CVD of graphene on commercial Cu foil using benzene as a precursor at the growth temperature of 400–1000 °C. Contrary to the published reports, we did not observe graphene growth below 700 °C when experiments in a residue-free reactor were carried out. We attribute the literature finding of low-temperature graphene growth to the accidental growth of graphene during the Cu annealing at 1000 °C in the presence of unintentional benzene residues in the reactor. Moreover, high-quality polycrystalline graphene films could be grown in the temperature range of 825–1000 °C with the grain-size increasing from 1 to 20 μm with increasing the growth temperature. Finally, the gas transport across as-prepared millimeter-sized membranes confirmed that the graphene film was free of large pinhole defects, and the majority of vacancy defects in these films were molecular-sized, below 0.38 nm, leading to an attractive sieving of hydrogen. Overall, benzene-derived high-quality graphene grown at 900 °C could prove useful for a number of applications where the conventional 1000 °C CVD growth is a bottleneck.

Contributions

K.A. and M.H.K. designed the project. M.M. and M.H.K. performed the experiments and wrote the manuscript with K.A. All authors revised the manuscript. M.R. helped with the Raman analysis and participated in the discussions. S.H. and J.Z. assisted with the nanoporous carbon film transfer process and membrane testing. M.D. carried out the TEM characterization.

Notes

The authors declare no competing financial interest.

Acknowledgements

Authors acknowledge the host institution, EPFL, for generous support. This project was primarily funded by the Swiss National Science Foundation under the Assistance Professor Energy Grant (grant number: PYAPP2_173645). A part of the project was funded by the Swiss Competence Center of Energy Research – Efficiency in Industrial Process.

Appendix A. Supplementary data

Supplementary data to this article can be found online at https://doi.org/10.1016/j.carbon.2019.07.045.

References

[1] S. Bae, H. Kim, Y. Lee, X. Xu, J.-S. Park, Y. Zheng, J. Balakrishnan, T. Lei, H. Ri Kim, Y. Il Song, Y.-J. Kim, K.S. Kim, B. Özyilmaz, J.-H. Ahn, B.H. Hong, S. Iijima, Roll-to-roll production of 30-inch graphene films for transparent electrodes, Nat. Nanotechnol. 5 (2010) 574–578, https://doi.org/10.1038/nnano.2010.132.

[2] X. Li, A. Reina, X. Jia, J. Ho, D. Nezich, H. Son, V. Bulovic, M.S. Dresselhaus, J. Kong, W. Cai, J. An, S. Kim, J. Nah, D. Yang, R. Piner, A. Velamakanni, I. Jung, E. Tutuc, S.K. Banerjee, L. Colombo, R.S. Ruoff, Large-area synthesis of high-quality and uniform graphene films on copper foils, Science 324 (2009) 1312–1314.

[3] K. Celebi, J. Buchheim, R.M. Wyss, A. Droudian, P. Gasser, I. Shorubalko, J. Kye, C. Lee, H.G. Park, Atomically thin porous graphene, Science 344 (2014) 289–293, 80-.

[4] D. Jiang, V.R. Cooper, S. Dai, Porous graphene as the ultimate membrane for gas separation, Nano Lett. 9 (2009) 4019–4024, https://doi.org/10.1021/nl9021946.

[5] Z. Yuan, J.D. Benck, Y. Eatmon, D. Blankschtein, M.S. Strano, Stable, temperature-dependent gas mixture permeation and separation through suspended nanoporous single-layer graphene membranes, Nano Lett. 18 (2018) 5057–5069, https://doi.org/10.1021/acs.nanolett.8b01866.

[6] S.P. Koenig, L. Wang, J. Pellegrino, J.S. Bunch, Selective molecular sieving through porous graphene, Nat. Nanotechnol. 7 (2012) 728–732, https://doi.org/10.1038/nnano.2012.162.

[7] S. Huh, J. Park, Y.S. Kim, K.S. Kim, B.H. Hong, J.-M. Nam, UV/Ozone-Oxidized large-scale graphene platform with large chemical enhancement in surface-enhanced Raman scattering, ACS Nano 5 (2011) 9799–9806, https://doi.org/10.1021/nn204156n.

[8] A.W. Robertson, G.-D. Lee, K. He, C. Gong, Q. Chen, E. Yoon, A.I. Kirkland, J.H. Warner, Atomic structure of graphene subnanometer pores, ACS Nano 9 (2015) 11599–11607, https://doi.org/10.1021/acsnano.5b05700.

[9] J. Zhao, G. He, S. Huang, L.F. Villalobos, M. Dakhchoune, H. Bassas, K.V. Agrawal, Etching gas-sieving nanopores in single-layer graphene with an angstrom precision for high-performance gas mixture separation, Sci. Adv. 5 (2019), https://doi.org/10.1126/sciadv.aav1851 eaav1851.

[10] L. Wang, L.W. Drahushuk, L. Cantley, S.P. Koenig, X. Liu, J. Pellegrino, M.S. Strano, J. Scott Bunch, Molecular valves for controlling gas phase transport made from discrete ångström-sized pores in graphene, Nat. Nanotechnol. 10 (2015) 785–790, https://doi.org/10.1038/nnano.2015.158.

[11] M.S.H. Boutilier, D. Jang, J.-C. Idrobo, P.R. Kidambi, N.G. Hadjiconstantinou, R. Karnik, Molecular sieving across centimeter-scale single-layer nanoporous graphene membranes, ACS Nano 11 (2017) 5726–5736, https://doi.org/10.1021/acsnano.7b01231.

[12] S. Huang, M. Dakhchoune, W. Luo, E. Oveisi, G. He, M. Rezaei, J. Zhao,

D.T.L. Alexander, A. Züttel, M.S. Strano, K.V. Agrawal, Single-layer graphene membranes by crack-free transfer for gas mixture separation, Nat. Commun. 9 (2018) 2632, https://doi.org/10.1038/s41467-018-04904-3.
[13] P.R. Kidambi, M.S.H. Boutilier, L. Wang, D. Jang, J. Kim, R. Karnik, Selective nanoscale mass transport across atomically thin single crystalline graphene membranes, Adv. Mater. 29 (2017), 1605896, https://doi.org/10.1002/adma.201605896.
[14] J.-H. Choi, Z. Li, P. Cui, X. Fan, H. Zhang, C. Zeng, Z. Zhang, Drastic reduction in the growth temperature of graphene on copper via enhanced London dispersion force, Sci. Rep. 3 (2013) 1925, https://doi.org/10.1038/srep01925.
[15] J. Jang, M. Son, S. Chung, K. Kim, C. Cho, B.H. Lee, M.-H. Ham, Low-temperature-grown continuous graphene films from benzene by chemical vapor deposition at ambient pressure, Sci. Rep. 5 (2015) 17955, https://doi.org/10.1038/srep17955.
[16] Z. Li, P. Wu, C. Wang, X. Fan, W. Zhang, X. Zhai, C. Zeng, Z. Li, J. Yang, J. Hou, Low-temperature growth of graphene by chemical vapor deposition using solid and liquid carbon sources, ACS Nano 5 (2011) 3385–3390, https://doi.org/10.1021/nn200854p.
[17] P.R. Kidambi, C. Ducati, B. Dlubak, D. Gardiner, R.S. Weatherup, M.-B. Martin, P. Seneor, H. Coles, S. Hofmann, The parameter space of graphene chemical vapor deposition on polycrystalline Cu, J. Phys. Chem. C 116 (2012) 22492–22501, https://doi.org/10.1021/jp303597m.
[18] Y. Xue, B. Wu, L. Jiang, Y. Guo, L. Huang, J. Chen, J. Tan, D. Geng, B. Luo, W. Hu, G. Yu, Y. Liu, Low temperature growth of highly nitrogen-doped single crystal graphene arrays by chemical vapor deposition, J. Am. Chem. Soc. 134 (2012) 11060–11063, https://doi.org/10.1021/ja302483t.
[19] E. Lee, H.C. Lee, S.B. Jo, H. Lee, N.-S. Lee, C.G. Park, S.K. Lee, H.H. Kim, H. Bong, K. Cho, Heterogeneous solid carbon source-assisted growth of high-quality graphene via CVD at low temperatures, Adv. Funct. Mater. 26 (2016) 562–568, https://doi.org/10.1002/adfm.201504194.
[20] L. Jiang, T. Niu, X. Lu, H. Dong, W. Chen, Y. Liu, W. Hu, D. Zhu, Low-temperature, bottom-up synthesis of graphene via a radical-coupling reaction, J. Am. Chem. Soc. 135 (2013) 9050–9054, https://doi.org/10.1021/ja4031825.
[21] J. Zhang, J. Li, Z. Wang, X. Wang, W. Feng, W. Zheng, W. Cao, P. Hu, Low-temperature growth of large-area heteroatom-doped graphene film, Chem. Mater. 26 (2014) 2460–2466, https://doi.org/10.1021/cm500086j.
[22] K. Gharagozloo-Hubmann, N.S. Müller, M. Giersig, C. Lotze, K.J. Franke, S. Reich, Requirement on aromatic precursor for graphene formation, J. Phys. Chem. C 120 (2016) 9821–9825, https://doi.org/10.1021/acs.jpcc.6b01781.
[23] T. Wu, H. Shen, L. Sun, J. You, Z. Yue, Three step fabrication of graphene at low temperature by remote plasma enhanced chemical vapor deposition, RSC Adv. 3 (2013) 9544, https://doi.org/10.1039/c3ra23388j.
[24] Y. Zhang, W. Ren, Z. Jiang, S. Yang, W. Jing, P. Shi, X. Wu, Z.-G. Ye, Low-temperature remote plasma-enhanced atomic layer deposition of graphene and characterization of its atomic-level structure, J. Mater. Chem. C. 2 (2014) 7570–7574, https://doi.org/10.1039/C4TC00849A.
[25] J.I. Fujita, T. Hiyama, A. Hirukawa, T. Kondo, J. Nakamura, S.I. Ito, R. Araki, Y. Ito, M. Takeguchi, W.W. Pai, Near room temperature chemical vapor deposition of graphene with diluted methane and molten gallium catalyst, Sci. Rep. 7 (2017) 1–10, https://doi.org/10.1038/s41598-017-12380-w.
[26] T. Wu, G. Ding, H. Shen, H. Wang, L. Sun, Y. Zhu, D. Jiang, X. Xie, Continuous graphene films synthesized at low temperatures by introducing coronene as nucleation seeds, Nanoscale 5 (2013) 5456, https://doi.org/10.1039/c3nr00963g.
[27] R.K. Von, E. Wicke, Die Oberflaichendiffusion Yon Kohlendioxydin Aktiven Kohlen, 1941, p. 2, https://doi.org/10.1002/adfm/201707427.
[28] P.Y. Huang, C.S. Ruiz-Vargas, A.M. van der Zande, W.S. Whitney, M.P. Levendorf, J.W. Kevek, S. Garg, J.S. Alden, C.J. Hustedt, Y. Zhu, J. Park, P.L. McEuen, D.A. Muller, Grains and grain boundaries in single-layer graphene atomic patchwork quilts, Nature 469 (2011) 389–392, https://doi.org/10.1038/nature09718.
[29] G. He, M. Dakhchoune, J. Zhao, S. Huang, K.V. Agrawal, Electrophoretic nuclei assembly for crystallization of high-performance membranes on unmodified supports, Adv. Funct. Mater. 28 (2018) 1–8, https://doi.org/10.1002/adfm.201707427.
[30] J.W. Suk, A. Kitt, C.W. Magnuson, Y. Hao, S. Ahmed, J. An, A.K. Swan, B.B. Goldberg, R.S. Ruoff, Transfer of CVD-grown monolayer graphene onto arbitrary substrates, ACS Nano 5 (2011) 6916–6924, https://doi.org/10.1021/nn201207c.
[31] I. Ruiz, W. Wang, A. George, C.S. Ozkan, M. Ozkan, Silicon oxide contamination of graphene sheets synthesized on copper substrates via chemical vapor deposition, Adv. Sci. Eng. Med. 6 (2014) 1070–1075, https://doi.org/10.1166/asem.2014.1615.
[32] N. Lisi, T. Dikonimos, F. Buonocore, M. Pittori, R. Mazzaro, R. Rizzoli, S. Marras, A. Capasso, Contamination-free graphene by chemical vapor deposition in quartz furnaces, Sci. Rep. 7 (2017) 9927, https://doi.org/10.1038/s41598-017-09811-z.
[33] L.G. Cançado, A. Jorio, E.H.M. Ferreira, F. Stavale, C.A. Achete, R.B. Capaz, M.V.O. Moutinho, A. Lombardo, T.S. Kulmala, A.C. Ferrari, Quantifying defects in graphene via Raman spectroscopy at different excitation energies, Nano Lett. 11 (2011) 3190–3196, https://doi.org/10.1021/nl201432g.
[34] A.C. Ferrari, D.M. Basko, Raman spectroscopy as a versatile tool for studying the properties of graphene, Nat. Nanotechnol. 8 (2013) 235–246, https://doi.org/10.1038/nnano.2013.46.
[35] J.E. Zanetti, G. Egloff, The thermal decomposition of benzene, J. Ind. Eng. Chem. 9 (1917) 350–356, https://doi.org/10.1021/ie50088a009.
[36] C.-M. Sung, M.-F. Tai, Reactivities of transition metals with carbon: implications to the mechanism of diamond synthesis under high pressure, Int. J. Refract. Metals Hard Mater. 15 (1997) 237–256, https://doi.org/10.1016/S0263-4368(97)00003-6.
[37] P.R. Kidambi, D.D. Mariappan, N.T. Dee, A. Vyatskikh, S. Zhang, R. Karnik, A.J. Hart, A scalable route to nanoporous large-area atomically thin graphene membranes by roll-to-roll chemical vapor deposition and polymer support casting, ACS Appl. Mater. Interfaces 10 (2018) 10369–10378, https://doi.org/10.1021/acsami.8b00846.
[38] S.C. O'Hern, D. Jang, S. Bose, J.-C. Idrobo, Y. Song, T. Laoui, J. Kong, R. Karnik, Nanofiltration across defect-sealed nanoporous monolayer graphene, Nano Lett. 15 (2015) 3254–3260, https://doi.org/10.1021/acs.nanolett.5b00456.
[39] L.W. Drahushuk, M.S. Strano, Mechanisms of gas permeation through single layer graphene membranes, Langmuir 28 (2012) 16671–16678, https://doi.org/10.1021/la303468r.
[40] C. Sun, M.S.H. Boutilier, H. Au, P. Poesio, B. Bai, R. Karnik, N.G. Hadjiconstantinou, Mechanisms of molecular permeation through nanoporous graphene membranes, Langmuir 30 (2014) 675–682, https://doi.org/10.1021/la403969g.
[41] K.V. Agrawal, L.W. Drahushuk, M.S. Strano, Observation and analysis of the Coulter effect through carbon nanotube and graphene nanopores, Philos. Trans. R. Soc. A 374 (2016), 20150357, https://doi.org/10.1098/rsta.2015.0357.
[42] L. Wang, M.S.H. Boutilier, P.R. Kidambi, D. Jang, N.G. Hadjiconstantinou, R. Karnik, Fundamental transport mechanisms, fabrication and potential applications of nanoporous atomically thin membranes, Nat. Nanotechnol. 12 (2017) 509–522, https://doi.org/10.1038/nnano.2017.72.